Design, synthesis and preliminary evaluation of 18F-labelled 1,8-naphthyridin-, quinolin- and pyridin-2-one-3-carboxamide derivatives for PET imaging CB2 cannabinoid receptor

Giuseppe Saccomanni, ❸[a] *Giancarlo Pascali*❸,[b,c] *Sara Del Carlo,*[a] *Daniele Panetta,*[b] *Mariarosaria De Simone,*[b] *Simone Bertini,*[a] *Silvia Burchielli,*[d] *Maria Digiacomo,*[a] *Marco Macchia,*[a] *Clementina Manera,*[a]* *Piero A. Salvadori*[b]

Dipartimento di Farmacia, Università di Pisa, via Bonanno 6, 56126 Pisa, Italy

CNR Istituto di Fisiologia Clinica,Via Moruzzi, 1, 56124 Pisa, Italy

ANSTO LifeSciences, PO Box M34, Camperdown 2050, Australia

Fondazione Toscana G. Monasterio, Via Moruzzi, 1, 56124 Pisa, Italy

* To whom correspondence should be addressed. C.M.: phone, +390502219548; fax, +390502219605; e-mail: manera@farm.unipi.it.

❸ These authors equally contributed to the paper.

RECEIVED DATE (to be automatically inserted after your manuscript is accepted if required according to the journal that you are submitting your paper to)

[a] Dipartimento di Farmacia, Università di Pisa

[b] CNR Istituto di Fisiologia Clinica, Pisa

[c] ANSTO LifeSciences, Camperdown

[d] Fondazione Toscana G.Monasterio

Abstract

In the present work, we report the synthesis of new aryliodonium salts to obtain ^{18}F-labelled compounds whose corresponding unlabelled fluorinated derivatives showed to be CB2 cannabinoid receptor specific ligands with Ki values in the low nanomolar range and high CB2/CB1 selectivity. Two radiolabelled compounds, [^{18}F]**AF4** and [^{18}F]**CB91**, were successfully formulated for *in vivo* administration and their preliminary biodistribution was assessed with microPET/CT. [^{18}F]**AF4** was readily eliminated while [^{18}F]**CB91** presented a reasonable stability *in vivo* and a preferential extraction of the tracer in the tissues that constitutionally express CB2 cannabinoid receptor. The results obtained indicate [^{18}F]**CB91** as a possible candidate marker of CB2 cannabinoid receptor distribution and is worth of further development for its perspective use in assessing pathologies or diseases, in which the expression of this receptor is increased.

Keywords: cannabinoid, CB1 receptor, CB2 receptor, iodonium derivatives, radiofluorination, microfluidic system

1. Introduction

CB2 cannabinoid receptor (CB2R) belongs to the rhodopsin-like family class A of G-protein-coupled receptors (GPCRs) and constitutes, with CB1 cannabinoid receptor (CB1R), the restricted family of cannabinoid receptors (CBRs) [1].

Even if CB1R is expressed throughout the body, it is found in higher concentrations in the brain and its activation is mainly associated with psychotropic and behavioural actions of cannabinoid drugs [2]. The CB2R is expressed in peripheral cells and tissues derived from the immune system [1] even if some recent studies showed that CB2R has a limited central nervous system distribution. In pathological conditions, the CB2R can be up-regulated and recent studies have highlighted that neuroinflammation, e.g. related to neurodegenerative (e.g. Alzheimer's) or autoimmune disorders (multiple sclerosis), stroke, trauma or brain tumors can lead to an over-expression of CB2R [3]. Therefore, interest in developing Positron Emission Tomography (PET) radioligands for non-invasive imaging of the CB2R in neurological diseases and cancer, and in monitoring the therapeutic efficacy of new anti-inflammatory drugs is growing. A number of radioligands with affinity for the human CB2R for *in vitro* use are available. Non-selective cannabinoid radioligands such as [^{3}H]CP55,940 or [^{3}H]WIN55,212 are extensively used in binding analyses of the CB2 receptor [4]. Even if ^{18}F-labelled tracers are preferred for PET imaging due to the longer radionuclide half-life (109 min), the majority of papers dealing with CB2R utilizes ^{11}C-radioligands. Carbon-11 is a very short-lived positron emitting radionuclide (20 min half-life), and was used in the preparation of the first CB2-selective ligand, the dimethoxy-triaryl bis-sulfone [^{11}C]methoxy-Sch225336 [5]. Subsequently, other [^{11}C]-labelled compounds have been synthesized and tested in animals, such as [^{11}C]A-836339 [3] and [^{11}C]KD2 [6], and also in healthy volunteers, such as [^{11}C]NE40 [7]. Most of these radioligands were obtained by using ^{11}C-methylation reactions, usually on demethylated substrates. A similar alkylation-based approach has been extended to fluorine-18 in the synthesis of a dideuterofluoromethyl derivative of a new CB2 scaffold based on a triazine moiety [8]. The use of deuterium was conceived to achieve improved stability towards *in vivo*

defluorination. Indeed, this fact may represent a problem with ^{18}F-radiolabelled tracers based on alkylfluorides, as the bone seeking fluoride anion may be removed *in vivo* from the scaffold and jeopardize tracer exploitability in terms of image reading and subject exposure to unnecessary radiations. Extensive research has been dedicated to a novel class of 2-oxoquinoline derivatives [4, 9-12], which have been radiolabelled with either carbon-11 or fluorine-18. In the quest for an optimal ^{18}F-labelled CB2R tracer, other scaffolds, with different structures, have been synthesized and evaluated for the *in vivo* visualization of CB2R , such as the N-dichlorobenzoyl fluoroethoxyindole [^{18}F]FE-GW405833 [13]. To circumvent the *in vivo* defluorination of scaffolds being labelled via the ^{18}F-fluoroethylation reaction, the route to the synthesis of a more stable aromatic fluoride was attempted by using an aromatic nucleophilic substitution on a N-aryl-oxadiazolyl-proprionamide [14], designed to bear a deactivated aromatic ring and a trimethylammonium leaving group.

Although *in vitro* biological data of these radioligands were promising, unsatisfactory results were obtained *in vivo* because of metabolic instability [4, 13], poor solubility [12], and limited potential usefulness from biodistribution studies [5].

In a research program aimed at obtaining CB2R selective ligands [15, 16] we described the synthesis and pharmacological characterization of several fluorinated derivatives possessing the 1,8-naphthyridin-, quinolin- and pyridin-2-one- central scaffold [15, 16]. Among these, **CB91**, **VL22** and **AF4** (Figure 1) demonstrated to be CB2R specific ligands with Ki values in the low nanomolar range and high CB2/CB1 selectivity, while bearing the fluorine atom on the aromatic ring, which in principle should ensure high in vivo stability of the label.

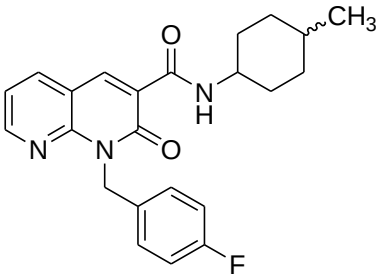

CB91; CB2R, Ki= 0.9 nM

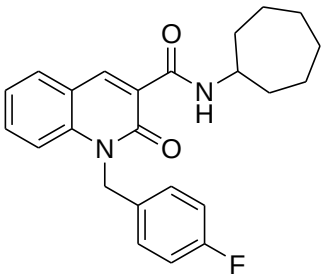

VL22; CB2R, Ki= 0.25 nM

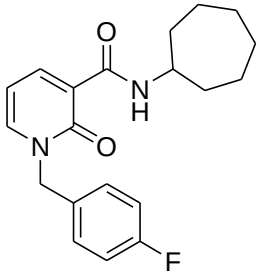

AF4; CB2R, Ki= 7.8 nM

Figure 1. Structures of fluorinated 1,8-naphthyridin- (**CB91**), quinolin- (**VL22**) and pyridin-2-one (**AF4**) derivatives.

As a general rule, the most convenient way of ^{18}F-labelling is to introduce the radionuclide in the final step of the synthetic process by using a nucleophilic substitution reaction [17]. In our case, we could not exploit the effect of electron-withdrawing groups, therefore an alternative route was identified in the use of aryliodonium salts [18], which represent a possible way to introduce a fluorine atom into an electron-rich aromatic ring. Hypervalent iodine bonded to two aromatics rings leads to the formation of a fluoroaryl and an iodoaryl derivative when reacted with fluoride: the former is usually generated on the less electron-rich ring.

In this work we report the synthesis of the aryliodonium salts of **CB91**, **VL22** and **AF4** and their radiofluorination in microfluidic conditions to obtain the corresponding ^{18}F-labelled compounds. [^{18}F]**AF4** and [^{18}F]**CB91**, whose corresponding unlabelled derivatives show promising clogP value and good Papp value for intestinal and blood-brain barrier (BBB) permeability, were also tested in microPET to assess their *in vivo* biodistribution in rodents.

2. Results and discussion

2.1. Synthesis and radiosynthesis.

Incorporation of ^{18}F into aryliodonium salts occurs preferentially on the less electron-rich ring. Therefore, aryliodonium salts bearing a thienyl portion were developed in order to direct the fluorination

towards the relatively deactivated benzylic group. Precursors were synthesised by reaction of a boronic acid and a diacetoxyiodo derivative in the presence of a suitable organic acid.

In a first attempt, the boronic derivative **2** was prepared by reaction of carboxamide **1** [16] with 4-(bromomethyl)phenyl boronic acid (Scheme 1). Then, the boronic acid **2** was reacted with 2-(diacetoxyiodo)thiophene, synthesized according to a published method [19]. Unfortunately this approach was unsuccessful in obtaining the desired derivative **3**. This phenomenon could be related to electron rich character of thiophene: an high level of impurities and side-products might originate from internal redox processes and other side-reactions of the highly reactive 2-(diacetoxyiodo)thiophene [20].

The synthetic approach was then modified creating the diacyloxy function on the benzylic portion which was reacted with the commercially available thienyl boronic acid (Scheme 2). This synthetic route was then successfully applied for the synthesis of all the designed precursors. As reported in Scheme 2 the N1-alkylation of carboxamides **1, 4** and **5** [15, 16] was performed in anhydrous THF/DMF with *p*-iodobenzylbromide in presence of NaH at room temperature and afforded the desired iodobenzyl derivatives **6, 7** and **8**. Oxidation of the iodine atom with $NaBO_3 \cdot 4H_2O$ led to the corresponding diacetoxyiodo derivatives. These compounds are characterized by high reactivity/instability and therefore they were not isolated and rapidly reacted with the 2-thienylboronic acid in presence of a Lewis acid (trifluoroacetic acid) to obtain the desired iodonium salts **3, 9** and **10** [21].

Scheme 1

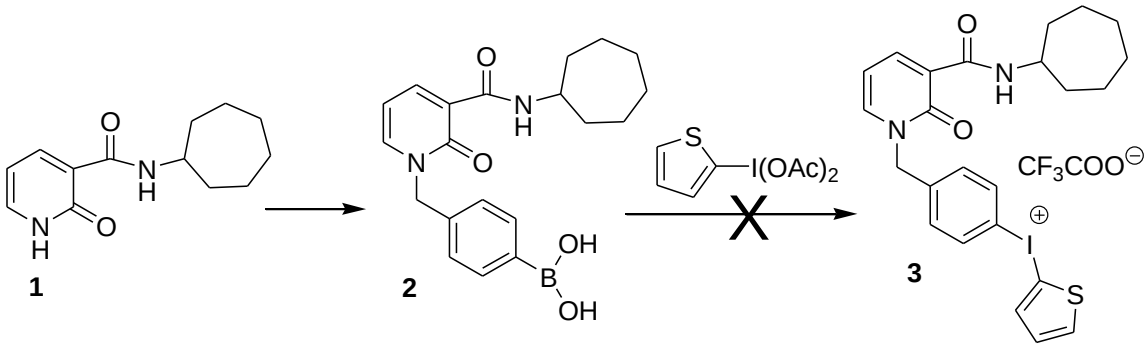

Scheme 2

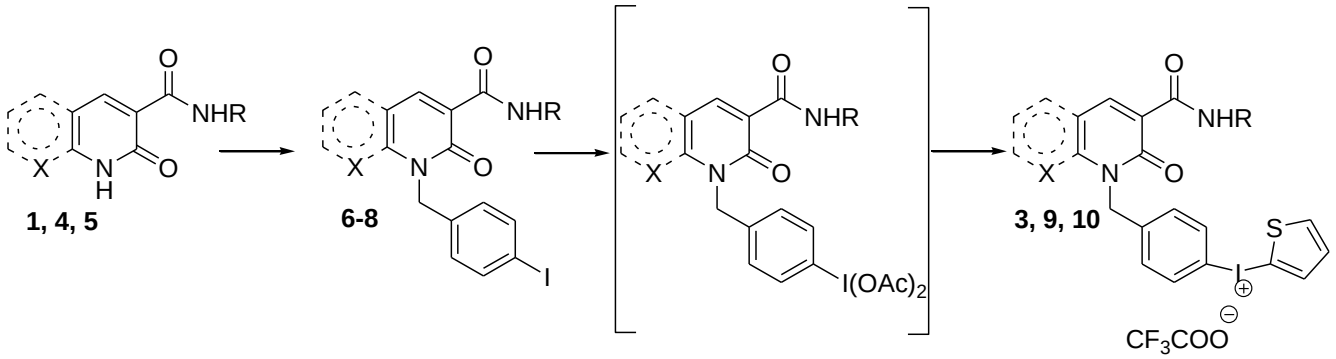

Name	Central scaffold	X	R
1, 6, 3	pyridin-2-one	--	Cycloheptyl
4, 7, 9	quinolin-2-one	CH	Cycloheptyl
5, 8, 10	naphthyridin-2-one	N	4-methylcyclohexyl

The aryliodonium salts **3**, **9** and **10** were radiolabelled, following classical nucleophilic fluorination conditions, by using potassium ^{18}F-fluoride/kryptofix (K_{222}) complex in DMSO (Scheme 3). The radiofluorination was optimized employing an Advion Nanotek microfluidic system; this apparatus allows delivering discrete amounts of both aryliodonium DMSO solution and the radiofluorinatinon complex, prepared using the traditional azeotropic distillation [21, 22], into a tubular flow reactor of 15.6 μL internal volume. Radiofluorination conditions were optimized by modifying reaction temperature, reagent relative ratios and residence time in microreactor by employing the minimum amount of precursor [23] The system used was also modified in order to perform the whole production process, and comprised an automated HPLC purification and a SPE processing to achieve the final injectable formulation [22].

Scheme 3

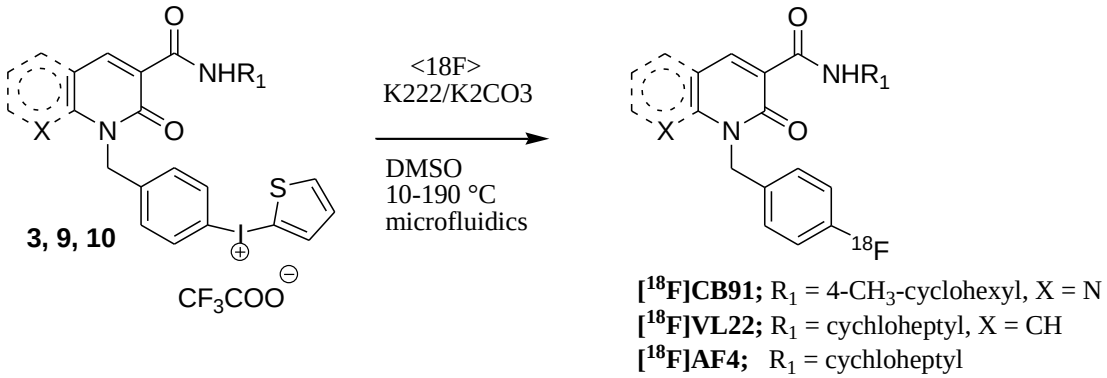

[^{18}F]CB91; R_1 = 4-CH_3-cyclohexyl, X = N
[^{18}F]VL22; R_1 = cychloheptyl, X = CH
[^{18}F]AF4; R_1 = cychloheptyl

Thus, the iodonium salt **3** was labelled to [^{18}F]**AF4** with a maximum 43±5% (n = 5) incorporation yield, by using a 40 μL/min overall flow at 190°C. These conditions were also optimal for the radiolabelling of the iodonium salt **10** to [^{18}F]**CB91**, which was obtained in 42±7% (n = 5) incorporation yield. Conversely, the iodonium salt **9** gave the corresponding labelled compound [^{18}F]**VL22** with only 3% yield (n = 10). The reason for the low yield reported with this last substrate is still unknown, and studies are on-going to clarify this result.

All purified products had high radiochemical purity (> 95%) and have been formulated in 10% ethanol/saline. However, the HPLC analysis of the reaction mixtures highlighted the presence of a secondary, unexpected non-radioactive peak [21]. The reduction of an iodonium salt precursor, occurring as a side reaction during ^{18}F-radiofluorination, was already reported in the literature [24]. This hypothesis was confirmed by direct comparison of the HPLC retention time and MS fragmentation of the unknown peaks with an authentic sample of the deiodinated analogues of **6** and **8** [21] thus confirming that this side reaction should be taken into account when using aryliodonium salts and considered during final product work up and in vivo utilization, the latter for possible unexpected interference with tracer imaging performances.

2.2 LogP and in vitro prediction of intestinal and BBB permeability.

The logP values for **CB91** and **AF4** were calculated in silico as clog P using the OSIRIS Property Explorer software (Thomas Sander, Actelion Pharmaceuticals Ltd., Gewerbestrasse 16, 4123 Allschwil, Switzerland,). The results obtained (clog P = 2.95-3.03 for **CB91** and clogP =2.18-2.61 for **AF4)** indicated favorable lipophilic characteristics for both intestinal absorption and BBB permeability.

These hypotheses were tested by using drug-permeability assays in Caco-2 cell lines and in MDCKII-hMDR1 cell lines to estimate their intestinal absorption and BBB permeability respectively. The results for **AF4** (Papp value = 66.0 ± 13.2 nm/s and 111.8 ± 2.2 nm/s for intestinal and BBB permeability respectively) and those previously reported for **CB91** (Papp value = 29.6 ± 0.2 nm/s and 65.0 ± 0.3 nm/s for intestinal and BBB permeability respectively) [25] indicate that these compounds are characterized by a medium–high absorption from the intestine after oral intake and good permeability across the BBB by passive diffusion.

2.3. In vivo experiments

The experimental protocol was conducted in accordance with the D.L. 116/92, implementation of the directive EEC 609/86, regarding the protection and use of animals in scientific research, enforced at the time of the experiments.

Since [^{18}F]**AF4** and [^{18}F]**CB91** were obtained with good radiochemical yields and higher process stability, their *in vivo* biodistribution was assessed with dynamic PET imaging in rodents.

Whole-body PET images were acquired in each animal and time-activity curves (TAC) were derived from average counts in region of interests (ROI) drawn on PET images in correspondence of the principal organs (brain, liver, kidney, lungs, heart). At the end of the experiment, animals were sacrificed and principal organs harvested for radioactivity counting. Counts were normalised to the weight of the sample and the injected dose.

Preliminary findings from *in vivo* PET imaging demonstrate that both [^{18}F]**AF4** and [^{18}F]**CB91** are quickly cleared from blood via the hepatobiliary elimination route, as demonstrated by high liver accumulation of the tracers since the earliest timeframes and early presence of radioactivity in the upper tract of the small intestine. Relative uptake of radioactivity in spleen and pancreas could not be resolved *in vivo* due to high liver uptake. Remarkably, fluorine remained bound to the organic moiety, as demonstrated by the very low uptake in bones and joints, substantially free from tracer accumulation even at later time of the experiment.

Compound [^{18}F]**AF4** was much prone to hepatic catabolism and no significant accumulation could be detected by both PET and organ counting in peripheral organs with higher CB2R expression , except from the liver and brown adipose tissue (BAT) (Figure 2). Gut radioactivity was related to content and not to intestine wall uptake. Analysis of PET dynamic images was consistent with a quick hepatic metabolism (Figure 3).

[^{18}F]**CB91** had a more complex pattern of distribution (Figure 4), showing also uptake in CB2R rich organs, such as the spleen and the gut wall, but also in other districts, like kidneys, pancreas and brown adipose tissue (BAT). PET findings have been confirmed by ex vivo organ counting (Figure 5); in particular, counts in urine were very low, thus demonstrating that the tracer binds to the kidney parenchyma but is not eliminated via this route.

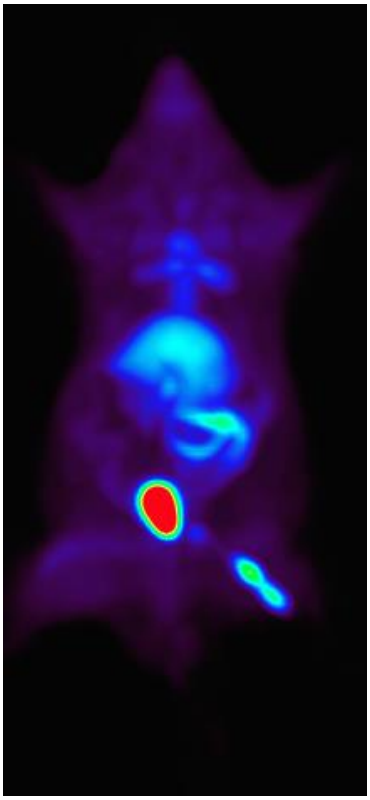

Figure 2. PET image of **[^{18}F]AF4** in vivo distribution**.** Tracer uptake in the liver and brown adipose tissue (BAT) is followed by rapid enteric and urinary elimination. Lower-left hot-spot in the picture corresponds to injection site.

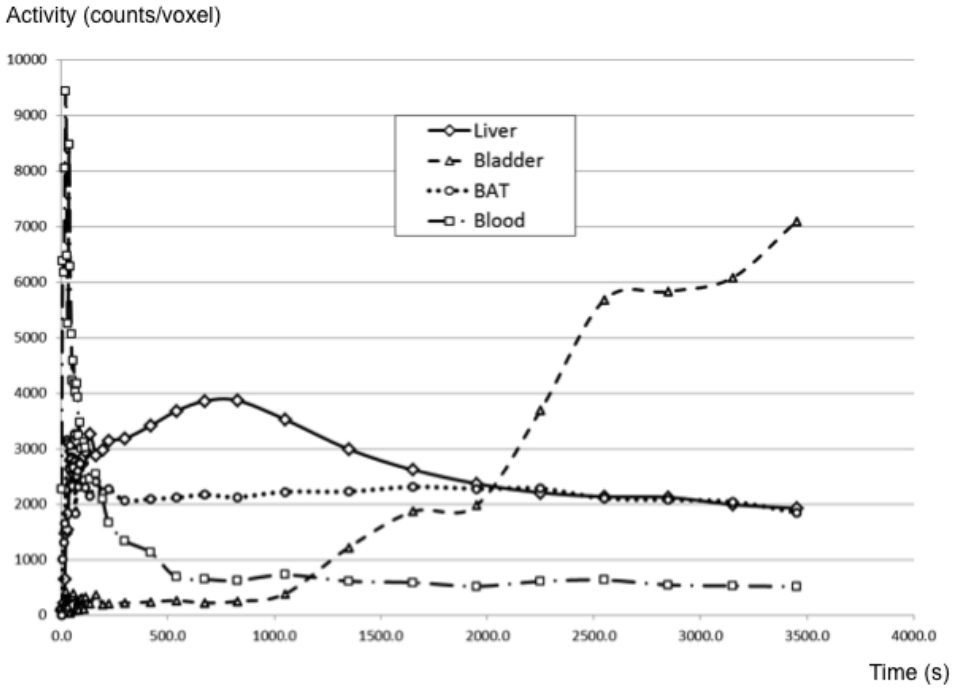

Figure 3. [^{18}F]AF4 in vivo kinetics. The rapid extraction by the liver is followed by enteric and urinary elimination of metabolites.

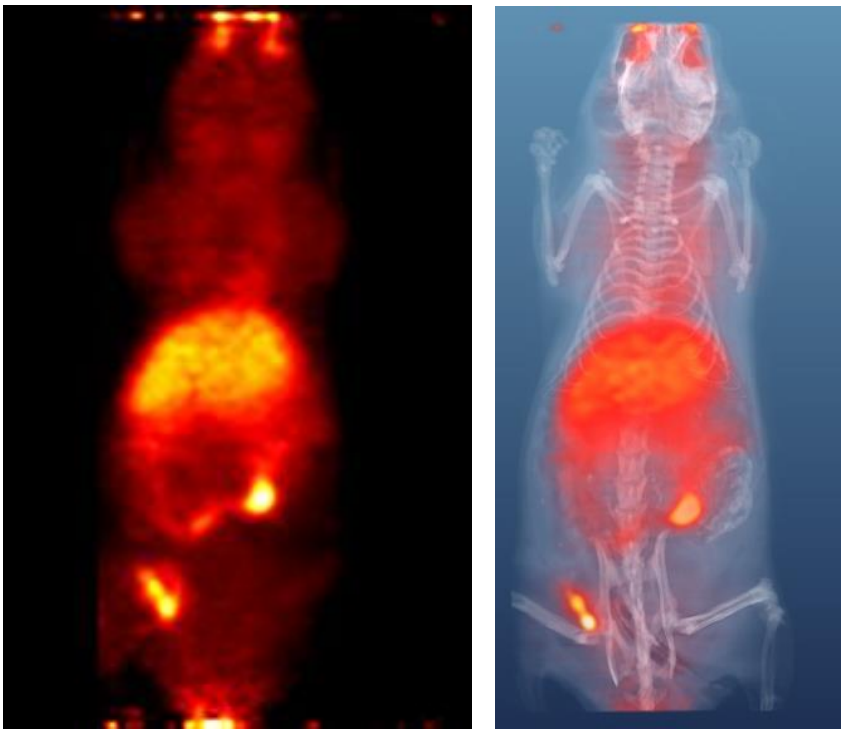

Figure 4. microPET/CT image of **[^{18}F]CB91** in vivo distribution (microPET image left panel, microPET and microCT fused images, right panel). A more widespread distribution can be observed with higher extraction in the liver, the gut, and kidneys. The absence of signal from the bladder indicates low urinary elimination.

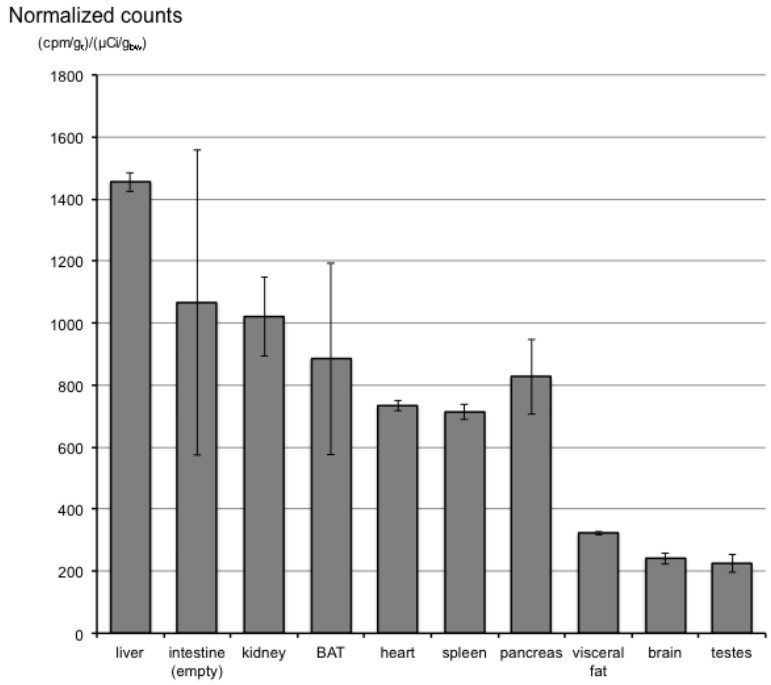

Figure 5. [^{18}F]CB91 ex vivo preliminary biodistribution data.

3. Conclusion

In the present work, starting from our high-affinity ligands **CB91**, **VL22** and **AF4**, [15, 16] we designed and synthesized three novel aryliodonium salts possessing chemical features amenable to ^{18}F-labelling.

An *ad hoc* microfluidic approach was developed for the radiolabelling, which led to good ^{18}F-incorporation yields for two of the three aryliodonium salts. Chemical and radiochemical purity were thoroughly assessed, highlighting that the concurrent reduction of iodonium salts during fluorination should be always considered for the possible generation of by-products.

[^{18}F]**AF4** and [^{18}F]**CB91** were successfully formulated for *in vivo* administration and preliminary pharmacokinetics evaluation with microPET/CT.

While [^{18}F]**AF4** turned out to be readily catabolised *in vivo*, [^{18}F]**CB91** showed a reasonable stability *in vivo* and a preferential extraction of the tracer in the tissues that constitutionally express CB2R but not in the brain. No *in vivo* defluorination was observed with [^{18}F]**CB91**.

Studies are on-going to demonstrate the specific binding of the tracer to the receptor and to further explore the perspective use of [^{18}F]**CB91** as biomarker of CB2R in pathologies or disease, including cancer, in which CB2R expression is increased.

4. Experimental

4.1. Chemistry

Reagents were purchased from commercial sources, and used without further purification. Melting points were determined on a Kofler hot stage apparatus and are uncorrected. ^{1}H NMR and ^{13}C NMR spectra were recorded with a Bruker AC–200 spectrometer. ^{1}H and ^{13}C chemical shifts are reported in δ units (ppm) downfield relative to the chemical shift for tetramethylsilane. Abbreviations s, d, t, and m denote singlet, doublet, triplet, and multiplet, respectively. Merck silica gel 60 was used for flash chromatography (230 − 400 mesh). The chemical purity of the target compounds was determined under the following conditions: the HPLC system was an LC Workstation Prostar (Varian, Inc., Walnut Creek, CA, USA) consisting of high pressure mixer pump (ProStar, model 230), DAD detector (ProStar, model 330) and a loop of 20 µl. Data were processed by a Star LC Workstation (Varian, Inc.). Chromatographic separation was performed on a Luna C_{18} ODS_2 analytical column (150 x 4.6 mm inner diameter, 3 µm particle size, Phenomenex, Torrance, CA, USA) maintained at 25° C. The mobile phase consisted of acetonitrile:water. Wavelengths were set at 220 and 320 nm. The purity of each compound was >96% in either analysis.

*4.1.1 4-{[3-(cycloheptylcarbamoyl)-2-oxopyridin-1(2h)-yl]methyl}phenylboronic acid (**2**).* To a solution of N-cycloheptyl-2-hydroxypyridine-3-carboxamide (**1**) (0.36 g, 1.54 mmol) in 10.0 ml of anhydrous THF, NaH (1.8 mmol, 60% in mineral oil) was added. After 1h, 2.5 ml of anhydrous DMF were added and a solution of 4-(bromomethyl)phenylboronic acid (0.39 g, 1.8 mmol) in 3.0 ml of anhydrous THF was dropped. The mixture was stirred for 24 h at room temperature. After the solvent was evaporated *in*

vacuo and the semisolid obtained was treated with water and pH was adjusted to 4-5 with diluted hydrochloride acid. After filtration the solid obtained was triturated with petroleum ether (40-60°C) and collected by filtration (80%), mp: 113-115°C, ^{1}H-NMR: $CDCl_3$ δ 9.93 (d, 1H, NH); 8.49 (d, 1H, H_4); 7.83 (d, 1H,Ar); 7.48 (d, 2H, H_6); 7.26 (d, 2H, Ar); 6.40 (m, 1H, H_5); 5.97 (s, 2 H, OH); 5.23 (s, 2H, CH_2); 4.12 (s, 1H, NCH); 1.85-1.30 (m, 12H, cycloheptyl).

4.1.2 General procedure for the synthesis of p-iodobenzyl derivatives.

The *p*-iodobenzyl derivatives **6-8** were obtained following the method previously reported [21]. Briefly to a solution of 1.0 mmol of the appropriate carboxamide **1, 4** and **5** in 10.0 mL of anhydrous THF, 1.2 mmol of NaH was added. After 1 hour at room temperature, 2.5 mL of anhydrous DMF and a solution of *p*-iodobenzylbromide (l.0 mmmol) in 3 mL of anhydrous THF were added. The mixture was stirred for 24 hours at room temperature and then was concentrated under reduced pressure treated with water and extracted with CH_2Cl_2. The organic layer was washed with brine, dried over anhydrous sodium sulfate, and evaporated to give a residue which was purified by crystallization.

*4.1.2.1. 1-(p-Iodobenzyl)-N-cycloheptyl-1,2-dihydro-2-oxopyridin-3-carboxamide (**6**).* Purified by crystallization from diisopropyl ether. Pale yellow powder (yield 86%); mp: 88-90°C; ^{1}H-NMR **(**DMSO) δ 9.71 (d, 1H, NH); 8.36 (m, 1H, Ar); 8.18 (m, 1H, Ar); 7.72 (d, 2H, Ar); 7.46 (d, 2H, Ar); 6.57 (m, 1H, Ar); 5.19 (s, 2H, CH_2); 3.90 (m, 1H, NCH); 1.81-1.44 (m, 12H, cycloheptyl). ^{13}C-NMR (DMSO) δ 162.44; 162.20; 143.81; 140.26; 138.36 (2C); 135.38; 130.00 (2C); 122.54; 107.25; 94.30; 52.48; 50.73; 35.20 (2C); 28.41(2C); 24.51 (2C).

*4.1.2.2. 1-(p-Iodobenzyl)-N-cycloheptyl-1,2-dihydro-2-oxo-quinolin-3-carboxamide (**7**).* Purified by crystallization from diisopropyl ether.Yellow powder **(**yield 50%**);** mp: 83-85°C ; ^{1}H-NMR **(**$CDCl_3$) δ 9.79 (d, 1H, NH); 9.00 (s, 1H, Ar); 7.81 (d, 2H, Ar); 7.68-7.53 (m, 3H, Ar); 7.35-7.22 (m, 2H, Ar); 6.95 (d, 2H, Ar); 5.56 (s, 2H, CH_2); 4.21 (m, 1H, NCH); 2.20-1.40 (m, 12H, cycloheptyl). ^{13}C-NMR ($CDCl_3$)

δ 162.39 ; 162.09 ; 144.41; 140.06, 138.24 (2C), 135.58, 132.95, 131.20, 128.54 (2C); 123.50; 122.04,120.32, 115.07; 93.08; 50.80, 46.17; 35.07 (2C), 28.34 (2C), 24.38 (2C).

*4.1.2.3. 1-(p-Iodobenzyl)-N-(4-methylcyclohexyl)-1,2-dihydro-2-oxo-1,8-naphthyridin-3-carboxamide (**8**).* Purified by crystallization from petroleum ether (100-140°C).Yellow powder **(**yield 73%)**;** mp: 84-86°C ; ^{1}H-NMR **(**DMSO) δ 9.80 and 9.42 (2d, 1H, NH); 8.95 (s, 1H, Ar); 8.73 (m, 1H, Ar); 8.52 (m, 1H, Ar); 7.62 (d, 2H, Ar); 7.45 (m, 1H, Ar); 7.05 (d, 2H, Ar); 5.66 (s, 2H, CH_2); 4.11 and 3.71 (m, 1H, NCH); 1.89-0.83 (m, 12H, cyclohexyl + CH_3). ^{13}C-NMR (DMSO) δ 161.49 ; 160.29 ; 151.77; 148.45 ; 141.75; 138.90; 136.45 (2C); 128.90 (2C); 121.90; 119.08; 115.64; 114.08; 92.17; 47.53; 44.14; 43.28; 32.87 (2C); 31.76 (2C); 30.77; 29.86; 29.17 (2C); 28.52 (2C); 21.52; 20.91.

4.1.3. General synthesis of p-iodobenzyl-(2-thienyl)-iodonium trifluoacetate derivatives.

The *p*-iodobenzyl-(2-thienyl)-iodonium trifluoacetate derivatives **3**, **9** and **10** were obtained following the method previously reported [21]. Briefly to a solution of 1 mmol of p-iodobenzyl derivatives **6, 7** or **8** in 40 mL of glacial acetic acid, 12 mmol of $NaBO_3 \cdot 4H_2O$ were added portionwise and under nitrogen atmosphere. The reaction mixture was stirred at room temperature for 30 minutes and then heated at 65 °C for 4 hours for compounds **6** and **7** and at 85 °C for 24 hours for compound **8**. After cooling, toluene was added and the azeotropic mixture was evaporated under reduced pressure. The obtained residue was treated with water and extracted with $CHCl_3$ for three times. The combined organic layers were dried over anhydrous sodium sulfate and evaporated to give a residue which was used for the next reaction step without further purification.

2.0 mmol of trifluoroacetic acid was added dropwise to a stirred solution of the above obtained residue in 10.0 mL of CH_2Cl_2 at -30°C. After 30 minutes the mixture was allowed to reach to room temperature and stirred for 1 hour. Then, the mixture was cooled at -30°C and 1.0 of 2-thienylboronic acid was added and stirred at room temperature for 16 hours. The reaction mixture was treated with diethyl ether to obtain the desired pure derivative **3**, **9** and **10** as white powder.

*4.1.3.1. {p-[1-(Benzyl)-N-cycloheptyl-1,2-dihydro-2-oxopyridin-3-carboxamide]}(2-thienyl) iodonium trifluoroacetate (**3**)*. White powder (yield 34%); mp: 80-83°C. ^{1}H-NMR (DMSO) δ 9.63 (d, 1H, NH); 8.35-7.95 (m, 6H, Ar+Th); 7.36 (d, 2H, Ar); 7.16 (m, 1H, Th); 6.58 (m, 1H, Ar); 5.27 (s, 2H, CH_2); 3.93 (m, 1H, NCH); 1.90-1.30 (m, 12H, cycloheptyl). ^{13}C-NMR **(**DMSO) δ 160.87; 160.70; 142.83; 142.45; 140.26; 139.71; 136.62; 134.20 (2C); 129.70 (2C); 128.97; 119.99; 117.45; 106.12; 100.42; 51.31; 48.85 (2C); 33.69 (2C); 26.97 (2C); 23.00 (2C);

*4.1.3.2. {p-[1-(Benzyl)-N-(4-methylcyclohexyl)-1,2-dihydro-2-oxo-quinolin-3-carboxamide]}(2-thienyl)iodonium trifluoroacetate (**9**).* White powder: (yield 20%); ^{1}H-NMR (DMSO) δ 9.70 (d, 1H, NH); 8.93 (s, 1H, Ar); 8.20-7.00 (m, 11H, Ar); 5.66 (s, 2H, CH_2); 4.03 (2m, 1H, NCH); 2.00-1.3 (m, 12H, cycloheptyl). ^{13}C-NMR (DMSO) δ 161.56; 161.33; 160.33; 151.71; 148.40; 141.90; 140.93; 139.68; 138.93; 136.98; 134.00(2C); 129.35; 128.95 (2C); 121.98; 119.17; 116.59; 114.22; 100.27; 47.51; 44.16; 43.50; 32.88 (2C); 31.72 (2C); 30.79; 29.85;29.15 (2C); 28.48 (2C); 21.52; 20.90

*4.1.3.3. {p-[1-(Benzyl)-N-(4-methylcyclohexyl)-1,2-dihydro-2-oxo-1,8-naphthyridin-3-carboxamide]}(2-thienyl)iodonium trifluoroacetate (**10**).* White powder: (yield 62%); mp: 98-100 °C. ^{1}H-NMR (DMSO) δ 9.72 and 9.35 (2d, 1H, NH); 8.97 (s, 1H, Ar); 8.70 (m, 1H, Ar); 8.56 (m, 1H, Ar); 8.18 (d, 2H, Ar); 8.05 (d, 1H, Th); 7.96 (d, 1H, Th); 7.45 (m, 1H, Ar); 7.35 (d, 2H, Ar); 7.17 (m, 1H, Th); 5.74 (s, 2H, CH_2); 4.09 and 3.73 (2m, 1H, NCH); 1.89-0.83 (m, 12H, cyclohexyl + CH_3). ^{13}C-NMR (DMSO) δ 161.56; 161.33; 160.33; 151.71; 148.40; 141.90; 140.93; 139.68; 138.93; 136.98; 134.00(2C); 129.35; 128.95 (2C); 121.98; 119.17; 116.59; 114.22; 100.27; 47.51; 44.16; 43.50; 32.88 (2C); 31.72 (2C); 30.79; 29.85;29.15 (2C); 28.48 (2C); 21.52; 20.90.

4.2. Radiochemistry

All chemicals and solvents were purchased from Sigma-Aldrich and used without further purification. The high-purity grade solvents were vented through a soda lime/molecular sieves trap upon use. Micro-SPE cartridges MP-1 were purchased from ORTG (USA). ^{18}F was produced at a PET trace cyclotron (GE Healthcare, USA) by proton bombardment (Ep= 16.7 MeV, 5-15 min at 20-25 μA) of a 1.3 mL 18O-water (enrichment > 98%) silver target. Radio-HPLCs were obtained using a Delta 600 pump system (Waters, USA) equipped with a Gabi Star flow-through gamma detector (Raytest, Germany) connected in series to a 996 Photo Diode Array (PDA) UV detector (Waters, USA) on a Phenomenex Synergi Hydro-RP 80A (4μm, 150x4,6mm) using varying CH_3CN/H_2O ratios. TLC analyses were performed using silica plates and 100% EtOAc as eluent. Radio-TLCs were acquired using a Cyclone PLUS (Perkin-Elmer, USA).

A general purpose Advion microfluidic system was used for optimizing key parameters of radiofluorination reactions (temperature, flow rate, reagents ratio), by employing the traditional 1-step Automatic Discovery setup described in literature [26]. When needed, semipreparative HPLC was run on a Phenomenex Synergi Fusion-RP 80A (4μm, 250x10mm) using varying CH_3CN/H_2O ratios.

4.2.1. Labelling experiments.

The aryliodonium precursor solution (10.0 mg of precursor in 0.5 mL of DMSO added with 3-5 mg of TEMPO and 50 μL of H_2O) was loaded into Pump 1 storage loop, while the fluorination complex, reconstituted in 0.7 mL of DMSO and prepared as previously reported [22], was loaded into Pump 3 storage loop. For optimization experiments, the two solutions were delivered in small boluses (10-50 μL) into a heated (130-190°C) fused silica microreactor of 15.6 μL internal volume at variable overall flow rate (20-100 μL/min). The obtained reaction mixtures were analysed by Radio-HPLC and/or Radio-TLC for assessing incorporation yield. Preparative scale runs (employing >100 μL fluoride

boluses) were performed utilizing optimized conditions; the reaction mixture was routed into the loop of a manual HPLC injection valve and injected into a semi-prep HPLC column. The product fraction (3-9 mL) was detected using a customized radioactivity probe and automatically diluted with 20 mL of H_2O. This solution was delivered to a Waters C-18 SepPack Plus for trapping the organic radiotracer, and the cartridge washed with additional 5 mL of H_2O to remove polar impurities. The desired product was eluted with 1.7 mL of EtOH, which was evaporated under a stream of nitrogen at 80°C. The residue was reconstituted with 200 μL of EtOH and 1.8 mL of saline, thus obtaining a preparation that could be used for animal injection or further analysis and characterization.

4.3. Animal treatment and imaging protocol

[^{18}F]**AF4** biodistribution was assessed in rats (Wistar, weighing approximately 250-280 g) using the ECAT EXACT HR+ scanner (CTI/Siemens, Knoxville TN, USA). Animals (n=3) were anaesthetised with i.p. administration of tiletamine/zolezepan and xylazine and deep anaesthesia was maintained throughout the study by inhalation of isoflurane (2% in oxygen). Once deep anaesthesia was achieved, the femoral vein was surgically isolated and a 24G catheter was inserted for radiotracer administration. After being positioned on the scanning couch, animals were administered with 25-30 MBq in 150-300 μl. The imaging protocol consisted in a dynamic whole-body scan with total acquisition time of 1 h and with the following framing: 5” (n=18), 10” (n=3), 30” (n=4), 120” (n=3), 150” (n=2), 300” (n=9). Images were reconstructed using filtered back-projection (FBP) with a voxel size of 2.57x2.57x2.42 mm^3,

[^{18}F]**CB91** biodistribution was assessed in mice (CD1). Animals (n=4) were anaesthetised with isoflurane (2% in oxygen) throughout the study. For a better assessment of tracer biodistribution and the anatomical identification of the organs, whole body PET scans were performed using the YAP-(S)PET micro-PET scanner (ISE srl, Vecchiano, Italy). In these cases, 6-8 MBq were injected in 100-150 μl in the tail vein and a dynamic micro-PET acquisition started upon injection for a total acquisition time of 1

hour, with the following framing: 60" (n=10), 120" (n=5), 300" (n=8). At the end of the dynamic micro-PET scan, a 15 minutes whole-body dynamic scan was performed. All micro-PET images were reconstructed using a model-based Ordered-Subset Expectation Maximization (OSEM) algorithm [27] with a voxel size of 0.75^3 mm^3. Subsequently, a whole body micro-CT (Xalt micro-CT scanner) [28], scan was performed (50 kVp, 0.7 mA, 3 min total scan time) without contrast agents. CT images were reconstructed using Feldkamp-type cone-beam FBP [29] with a voxel size of 74^3 μm^3 and then co-registered to the micro-PET images for anatomical reference.

4.4. In vitro prediction of intestinal permeability and BBB permeability.

The intestinal absorption and the of BBB permeability for compound **AF4** were determined according to the procedures reported for **CB91** [25]. For intestinal permeability the Caco-2 cell line was obtained from European Collection of Cell Culture (ECACC) and Madin Darby Canine Kidney cells stably transfected with the human MDR1 gene (MDCKII-hMDR1) were purchased by Netherlands Cancer Institute. For transport studies, 200,000 cells/well for Cawere seeded on Millicell 24-well cell culture plates. After 24 hours of incubation at 37 °C and 5% CO_2, the medium was changed with Enterocyte Differentiation Medium with additives (Becton Dickinson). The transport across the Caco-2 monolayer was determined from apical to basolateral side (A→B) by adding a 10 μM solution of test compound in DMEM (1% final concentration of DMSO) to the apical side. After 2 hours incubation period at 37 °C, 5% CO_2, the basolateral side solution, the apical and the starting solutions were analyzed and quantified by LC-MS/MS using verapamil as internal standard..

The BBB permeability was determined using MDCKII-hMDR1 assay as previously reported [25]. Madin Darby Canine Kidney cells stably transfected with the humanMDR1 gene (MDCKII-hMDR1) were purchased by Netherlands Cancer Institute. The transport across the monolayer MDCKII-hMDR1 was determined from apical to basolateral side (A→B) by adding a 10 μM solution of test compound in Dulbecco's Phosphate Buffered Saline (DPBS) (0.2% DMSO final concentration) to the apical side.

After 1 hour incubation at 37°C, 5%CO_2 the basolateral, the apical and the starting solutions were analyzed and quantified by LC-MS/MS using verapamil 0.1 µM as internal standard.

The samples were analyzed on UPLC (Waters) interfaced with a Premiere XE Triple Quadrupole (Waters). Mobile phases comprised 5% (v/v) acetonitrile in deionized water with 0.1% (v/v) formic acid (Phase A) and 5% (v/v) deionized water in acetonitrile with 0.1% (v/v) formic acid (Phase B). The column was Acquity BEH C18, 50x1mm 1.7 µm at 50 °C with flow of 0.25 ml/min (for intestinal permeability) or of 0.6 ml/min (for BBB permeability) and volume injection of 5 µl. The chromatographic method is the same previously report for compound **CB91** [25].Samples were analyzed in Multiple Reaction Monitoring conditions (MRM): electron spray ionization (ESI) positive, desolvation temperature 450 °C, desolvation gas 900 l/h, cone gas 50 l/h, collision gas 0.22 l/h. In particular for AF4 MRM: 343.18 → 109.05, 343.18 → 230.08; Cone Voltage: 32 V; Collision Energy: 16–34 eV.

The apparent permeability coefficient (Papp) (nm x s-1), was calculated as follows:

$$Papp = dQr/dt/ A \times C_0$$

dQr/dt is the cumulative amount in the receiver compartment versus time; A the area of the cell monolayer; C_0 the initial concentration of the dosing solution.

Acknowledgements

This work was performed under the PETALS II project, funded by ARISLA 2010 grant program

References.

[1] S. Munro, K. L.Thomas, M. Abu-Shaar, Nature 365 (1993) 61 − 65.

[2] L. A. Matsuda, S. J. Lolait, M. J.Brownstein, A. C.Young, T. I.Bonner, Nature 346 (1990) 561 − 564.

[3] A. G. Horti, Y. Gao, H. T. Ravert, P. Finley, H. Valentine, D. F. Wong, C. J. Endres, A. V. Savonenko, R. F. Dannals, Bioorg. Med. Chem. 18 (2010) 5202–5207

[4] N. Evens, G. G. Muccioli, N. Houbrechts, D. M. Lambert, A. M. Verbruggen, K. Van Laere, G. M. Bormans, Nucl. Med. Biol. 36 (2009) 455-465.

[5] N. Evens, B. Bosier, B. J. Lavey, J. A. Kozlowski, P. Vermaelen, L. Baudemprez, R. Busson, D. M. Lambert, K. Van Laere, A. M. Verbruggen, G. M. Bormans, Nucl. Med. Biol. 35 (2008) 793-800.

[6] L. Mu, D. Bieri, R. Slavik, K. Drandarov, A. Müller, S. Cermak, M. Weber, R. Schibli, S. D. Krämer, S. M. Ametamey, J. Neurochem. 126 (2013) 616-624.

[7] R. Ahmad, M. Koole, N. Evens, K. Serdons, A. Verbruggen, G. Bormans, K. Van Laere, Mol. Imaging Biol. 15 (2013) 384-390.

[8] L. Hortala, J. Arnaud, P. Roux, D. Oustric, L. Boulu, F. Oury-Donat, P. Avenet, T, Rooney, D. Alagille, O. Barret, G. Tamagnan, F. Barth, Bioorg. Med. Chem. 24 (2014) 283-287.

[9] K. H. Raitio, J. R. Savinainen, T. Nevalainen, T. Järvinen, J. Vepsäläinen, Chem. Bio. Drug Des. 68 (2006) 334-340.

[10] M. Gao, M. Wang, K. D. Miller, G. D. Hutchins, Q. H. Zheng, Bioorg. Med. Chem. 18 (2010) 2099-2106.

[11] N. Turkman, A. Shavrin, R. A. Ivanov, B. Rabinovich, A. Volgin, J. G. Gelovani, M. M. Alauddin, Bioorg. Med. Chem. 19 (2011) 5698-5707.

[12] N. Turkman, A. Shavrin, V. Paolillo, H. H. Yeh, L. Flores, S. Soghomonian, B. Rabinovich, A. Volgin, J. Gelovani, M. Alauddin, Nucl. Med. Biol. 39 (2012) 593-600.

[13] N. Evens, C. Vandeputte, G. G. Muccioli, D. M. Lambert, V. Baekelandt, A. M. Verbruggen, Z. Debyser, K. Van Laere, G. M. Bormans, Bioorg. Med. Chem. 19 (2011) 4499-4505.

[14] R. Teodoro, R. P. Moldovan, C. Lueg, R. Günther, C. K. Donat, F. A. Ludwig, S. Fischer, W. Deuther-Conrad, B. Wünsch, P. Brust, Org. Med. Chem. Lett. 3 (2013) 1-18.

[15] C. Manera, G. Saccomanni, B. Adinolfi, V. Benetti, A. Ligresti, M. G. Cascio, T. Tuccinardi, V. Lucchesi, A. Martinelli, P. Nieri, E. Masini, V. Di Marzo, P. L. Ferrarini, J. Med. Chem. 52 (2009) 3644-3651.

[16] C. Manera, G. Saccomanni, A. M. Malfitano, S. Bertini, F. Castelli, C. Laezza, A. Ligresti, V. Lucchesi, T. Tuccinardi, F. Rizzolio, M. Bifulco, V. Di Marzo, A. Giordano, M. Macchia, A. Martinelli, Eur. J. Med. Chem. 52 (2012) 284-294.

[17] L. Cai, S. Lu, V. W. Pike, Eur. J. Org. Chem. 17 (2008) 2853-2873.

[18] V.W Pike, F.J. Aigbirhio, J Chem Soc Chem Comm (1995) 2215-2216.

[19] H. Togo, T. Nabana, K. Yamaguchi, J. Org. Chem. 65 (2000) 8391-8394.

[20] M. A. Carroll, V. W. Pike, D. A. Widdowson, Tetrahedron Lett. 41 (2000) 5393-5396

[21] G. Pascali, S. Del Carlo, S. Rocchiccioli, G. Signore, G. Saccomanni, C. Manera, M. Macchia, P. A. Salvadori, J. Radioanal. Nucl. Chem. Submitted for pubblication.

[22] G. Pascali, A. Berton, M. DeSimone, N. Wyatt, L. Matesic, I. Greguric, P. A. Salvadori, Appl. Rad. Isotop. 84 (2014) 40-47.

[23] G. Pascali, L. Matesic, T.L. Collier, N. Wyatt, B.H. Fraser, T.Q. Pham, P.A. Salvadori, I. Greguric, Nature Protocols (2014) accepted for pubblication

[24] B.S. Moon, H.S. Kil, J.H. Park, J.S. Kim, J. Park, D.Y. Chi, B.C. Lee, S.E. Kim, Org. Biomol. Chem. 9 (2011) 8346-8355.

[25] A. M. Malfitano, C. Laezza, G. Saccomanni, T. Tuccinardi, C. Manera, A. Martinelli, E. Ciaglia, S. Pisanti, M. Vitale, P. Gazzerro, M. Bifulco, J.Neuroimmune. Pharmacol. 8 (2013) 1077-1086.

[26] G. Pascali, G. Mazzone, G. Saccomanni, C. Manera, P. A. Salvadori, Nucl. Med. Biol. 37 (2010) 547-555.

[27] S. Moehrs, M. Defrise, N. Belcari, A. D. Guerra, A. Bartoli, S. Fabbri, G. Zanetti, Phys. Med. Biol. 53 (2008), 6925-6945.

[28] D. Panetta, N. Belcari, A. Del Guerra, A. Bartolomei, P. A. Salvadori, Phys. Med. 28 (2012), 166-173.

[29] L. A. Feldkamp, L. C. Davis, J. W. Kress, J. Opt. Soc. Am. 1 (1984), 612-619